



Impact of High-Reactivity Advanced Test Reactor Experiments on Photon Heating in Nearby Experiment Locations

November 2024

Changing the World's Energy Future

Paul E Gilbreath, Michael Jason Worrall, Joseph W Nielsen, Gregory K Housley



DISCLAIMER

This information was prepared as an account of work sponsored by an agency of the U.S. Government. Neither the U.S. Government nor any agency thereof, nor any of their employees, makes any warranty, expressed or implied, or assumes any legal liability or responsibility for the accuracy, completeness, or usefulness, of any information, apparatus, product, or process disclosed, or represents that its use would not infringe privately owned rights. References herein to any specific commercial product, process, or service by trade name, trade mark, manufacturer, or otherwise, does not necessarily constitute or imply its endorsement, recommendation, or favoring by the U.S. Government or any agency thereof. The views and opinions of authors expressed herein do not necessarily state or reflect those of the U.S. Government or any agency thereof.

Impact of High-Reactivity Advanced Test Reactor Experiments on Photon Heating in Nearby Experiment Locations

Paul E Gilbreath, Michael Jason Worrall, Joseph W Nielsen, Gregory K Housley

November 2024

**Idaho National Laboratory
Idaho Falls, Idaho 83415**

<http://www.inl.gov>

**Prepared for the
U.S. Department of Energy
Under DOE Idaho Operations Office
Contract DE-AC07-05ID14517**

Impact of High Reactivity Advanced Test Reactor
Experiments on Photon Heating in Nearby Experiment
Locations

Paul E. Gilbreath,^{*,a} Michael J. Worrall,^a Joseph W. Nielsen,^a and Greg K.
Housley^a

^a*Idaho National Laboratory, 2525 Fremont Ave., Idaho Falls, ID 83406*

*Email: paul.gilbreath@inl.gov

Number of pages: 22
Number of tables: 6
Number of figures: 7

Abstract

The Advanced Test Reactor (ATR)'s distinctive ability to provide a wide range of irradiation conditions is attractive for programs pursuing fuel qualification experiments. These potentially high-fuel-load experiments are a relatively new development and produce unexplored effects on nearby experiments. This article explores how photon heating of such an experiment may affect other nearby experiment programs, ultimately serving to better inform decisions regarding experiment design and risks to programmatic goals. The Monte Carlo for the 21st Century (MC21) code is used to model and study how gamma heat generation rates (HGRs) and axial effects impact different ATR positions. The results reveal that the proximity of a given experiment's position to the high-fuel-load one can significantly alter that experiment's expected axial profile.

Keywords — Advanced Test Reactor, High Performance Research Reactors, Photon Heating

I. INTRODUCTION

The Advanced Test Reactor (ATR) promotes the advancement of nuclear science and technology by providing a unique selection of experiment positions for high neutron flux experiment irradiations in support of research and power reactors. With the current push to convert the U.S. High Performance Research Reactors (HPRR) from highly enriched uranium to low-enriched uranium (LEU), a wide assortment of fuel qualification efforts are being conducted, including the irradiation of experiments containing excessive amounts of fuel. ATR Reactor Engineering uses evaluation guidelines for experiments to ensure ATR safety. If an experiment contains more than 50 g of U-235 and/or a reactivity worth of more than 25 cents, additional safety actions must be taken, sometimes including validation using the Advanced Test Reactor Critical facility. The experiments we are considering significantly exceed these evaluation guidelines, in this case more than an order of magnitude. Since such high-fuel-load experiments are a relatively new development, beginning with the Ki-Jang Research Reactor (KJRR) fuel qualification experiment, there are some unexplored effects of these highly reactive experiments, particularly on nearby experiments.

Unintentional gamma heating poses a risk to nearby experiments by altering experimental conditions and potentially inducing temperature increases. Consequently, understanding the impact of these high-energy gamma rays is vital for ensuring the integrity of nearby experiments in the ATR.

The present article aims to provide some insights into the impacts that a high-fuel-load experiment may have on other nearby experiments. By using the Monte Carlo for the 21st Century (MC21) code to model and study these effects, nearby experiment programs can make better-informed decisions about experiment design and risks to programmatic goals.

Sec. II details the background information relevant to the current discussion. Sec. III provides information on the physics model, experimental setup, and analysis. Secs. IV and V present the results and overall conclusion, respectively.

II. BACKGROUND

II.A. Advanced Test Reactor

The ATR, depicted in Fig. 1, is a water-cooled 250 MW reactor that comprises a serpentine pattern of 40 fuel elements that create a four-leaf clover shape between a 3x3 array of flux trap regions. The 48-in. core is surrounded by a metallic beryllium reflector and 16 outer shim control cylinders (OSCCs), each containing a 120-degree arc of hafnium that can be rotated away from the core. Inside the four-leaf clover shape is the aluminum neck shim housing which contains 24 rods of hafnium for additional reactor control. The four leaves are referred to as lobes with a fifth lobe located in the center of the clover shape. By rotating the OSCCs, each lobe can be controlled to reach a different power, enabling a wide variety of potential irradiation conditions. The experiment positions are located within each flux trap, inside the neck shim housing, and throughout the beryllium reflector—a large assortment of experiment sizes.

A typical ATR cycle runs for 50–60 days at a total power of 110–120 MW. Depending on the parameters requested for a given experiment, lobe powers can be operated from about 16 to 30 MW and an appropriate ATR fuel load is designed to maintain power for the duration of the cycle. Typically, experiments located in flux traps or with very sensitive conditions will request the lobe powers while other experiments in smaller locations will satisfy design requirements by choosing locations conducive to meeting their programmatic goals. Experiments can range in complexity from “drop in” experiments, which are in contact with the primary coolant and sometimes contain a capsule of specimens, to loop experiments, which are hydraulically isolated to simulate various different conditions (e.g., specific pressures and coolant temperatures). Experiments can also contain fixed instrumentation such as flux wires, melt wires, or lead-in instruments (e.g., thermocouples and gas monitoring systems) in order to enable real-time measurements. As a result of the wide range of possible irradiation conditions, a variety of experiments can be accommodated, including materials tests, fueled experiments, isotope production, etc. (for more information, see [1]).

II.B. U.S. High Performance Research Reactors

The Department of Energy’s Material Management and Minimization program has been tasked with designing and qualifying conversion fuel for transitioning the five remaining HPRRs

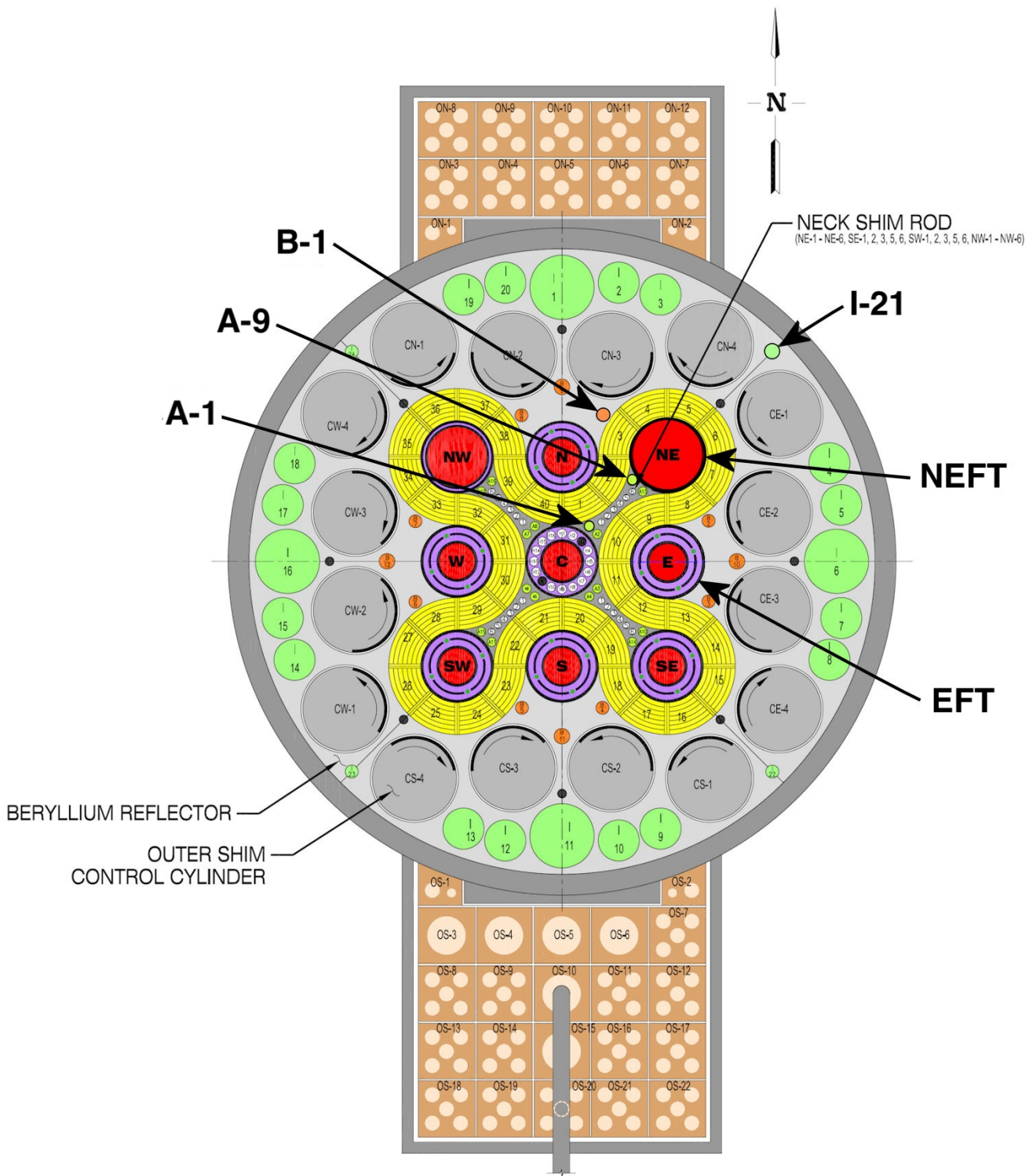


Fig. 1. ATR cross section.

from highly enriched uranium to LEU. An appropriate high-density LEU fuel does not already exist due to the high demands placed on HPRR fuels, so the HPRR Fuel Qualification Pillar will qualify a new fuel type, including commercialization of fuel fabrication. Qualification of this aluminum-clad, uranium alloyed with 10 wt% molybdenum (U-10Mo) monolithic fuel relies on appropriate irradiation testing and examination to ensure suitable performance for each of the HPRRs, as well as acceptance by the Nuclear Regulatory Commission. To make this assurance, various experiments have been conducted in the ATR and further experiments are planned.

These HPRR experiments encompass a full range of fuel region and cladding thicknesses that are representative of different fuel geometries and are specifically optimized to achieve operating conditions in support of fuel qualification for each reactor. They also utilize fuel plates ranging in size from miniplates (roughly 1x4 in.), which are used for fuel development and to ensure commercial fabricability, to full-sized plates and entire fuel elements (up to 1.5 kg U-235) for licensing the fuel system of each reactor. More information can be found in the U-10Mo Monolithic Fuel Qualification Plan [2]. By leveraging the large variety of experiment sizes and irradiation conditions, the irradiation needs of the HPRR program's fuel qualification plan can be solely provided by the ATR. Consequently, the larger experiments, particularly those inserted in the flux traps, could potentially impact nearby experiments to an extent that needs to be better understood.

II.C. Motivation

Starting in ATR cycle 158A in 2015, a first-of-its-kind experiment was irradiated to qualify the KJRR fuel. The experiment consisted of an entire U-7Mo LEU fuel element placed in the ATR's Northeast Flux Trap (NEFT) position and irradiated for four cycles. This fuel type was similar to the fuel described in Sec. II.B, with the important distinction that it was a dispersion fuel region instead of monolithic. More information can be found in KJRR validation report section on experiment description [3]. The ATR faced many challenges associated with this experiment, including the high reactivity worth of roughly 620 g of U-235 over only half the ATR's axial length. The experiment was so reactive that a similarly reactive backup (within 25 cents) was not available in case the experiment was not able to be inserted for irradiation, so two ATR fuel loadings per cycle had to be designed in order to accommodate the cycle length and power requirements. In regard to the ATR fuel elements, extra precautions had to be taken to account for the axial flux

profile deviation associated with such a large amount of fuel in only the axial central half of the reactor [4].

Potential considerations were not limited to ATR reactor safety and operations. One nearby lead-in instrumented experiment reported elevated heat rates which were concluded to be partially associated with the KJRR-caused axial perturbation of the ATR flux profile. This experiment used line-in thermocouples to monitor and appropriately change gas compositions to reflect programmatic temperature goals. This experiment program decided to remove their experiment for the remainder of the KJRR cycle irradiations due to the added uncertainty involved [5].

As a result of future HPRR experiments being planned for insertion into the ATR NEFT, some experiment programs are concerned about the potential effects and risks that these higher reactivity experiments pose to nearby experiment positions. The purpose of the present article is to better inform programmatic decisions regarding nearby experiments—both in terms of these irradiations as well as future similarly uranium-loaded and reactive experiments.

III. METHODOLOGY

III.A. Model Description

This analysis was performed using MC21, a continuous-energy Monte Carlo neutron and photon transport code which enables three dimensional modeling of steady-state problems [6]. All complex problem-dependent specifications such as geometry, material specifications, and tallies were prepared using the Physics Unified Modeling and Analysis Application Programming Interface (PUMA-API) which generates MC21 input via Java files. Employing the PUMA-API enabled the experiment configurations explored in this article to be easily used, in an object-oriented fashion, alongside a prepared modular base model of the ATR [7].

The MC21 code and ATR model have limited documented external validation efforts, but one case does address model benchmarking using burnup data from a different LEU U-Mo experiment [8].

The Evaluated Nuclear Data File B-VIII [9] continuous cross-section data were utilized for this analysis. The temperatures of all the materials, including the ATR driver fuels, were defined uniformly by setting an ambient temperature of 300 K. All spatial calculations were based on the fully coupled neutron-photon transport mode, which explicitly performs prompt/delayed neutron

and photon transport. The detailed photon transport is performed subsequent to the neutron transport by using recorded photon source information including position, energy, and direction.

III.B. Experimental Setup

The experiment setup for this work consists of a homogenized version of the University of Missouri Research Reactor (MURR) Design Demonstration Element (DDE). MURR-DDE was designed for generic fuel qualification and licensing of the U-10Mo monolithic fuel for the LEU conversion of the prototypic MURR core. The experiment is a slightly modified MURR 19.75% enriched LEU fuel element containing 23 curved fuel plates, positioned within an aluminum basket, and located in the ATR NEFT. The active fuel length is 24 in., and the total element contained about 1.5 kg of U-235. This element was designed to meet the programmatic power density and fission density targets of its limiting plates [10].

The particular model for this work was set up to homogenize the element itself. The fuel plates, structural side plates, and water channels have been homogenized into a single region for ease of experimental setup perturbations. Though insufficient for MURR-DDE experiment analyses, this simplification was assumed sufficient to reveal the gamma heating effects on nearby experiments. The perturbations include slightly changing the axial location of the element, removing hafnium flux shaping collars which tailor the axial flux to be consistent with the actual experiment's programmatic goals, changing the axial length (and therefore amount of fuel), and changing the fuel density. The perturbations, along with their relevant details, can be found in Table I. While the primary intention was to compare the effects of the MURR-DDE to sans MURR-DDE, the other configurations are meant to shed light on prospective high-load experiments that have yet to be designed or analyzed.

The ATR's Large Irradiation Housing Assembly (LIHA) model was used as a baseline for comparison. The LIHA is an aluminum basket with 23 equally sized smaller positions containing four large irradiation facility flux monitor holders, 10 Al fillers, and nine cobalt capsules. This LIHA configuration is well known for the ATR and the potential backup for the MURR-DDE experiment, though unsurprisingly not reactivity equivalent. Both the LIHA and the homogeneous MURR-DDE experiment configurations are depicted in Fig. 2.

TABLE I
Model configurations for the ATR NEFT.

Configuration	Mass U-235 [kg]	Axial Location	Notes on Perturbation
liha	0	n/a	The Large Irradiation Housing Assembly (LIHA) containing 4 flux monitor holders, 10 Al fillers, and 9 cobalt capsules.
homogenHf	1.5	+2.5 in.	The homogenized MURR-DDE experiment. For programmatic axial neutron flux profile shaping, it is centered at +2.5 in. of core centerline and contains additional hafnium collars.
homogen	1.5	+2.5 in.	Like “homogenHf,” but without the hafnium collars.
centered	1.5	center	Like “homogen,” but centered at core centerline, not at +2.5 in.
halfHomogen	0.75	+2.5 in.	Like “homogen,” but the homogenized fuel element is half the length.
halfCent	0.75	center	Like “centered,” but the homogenized fuel element is half the length.
halfDens	0.75	center	Like “centered,” but half the uranium density.
halfDensHalfLen	0.375	center	Like “halfDens,” but half the uranium density.

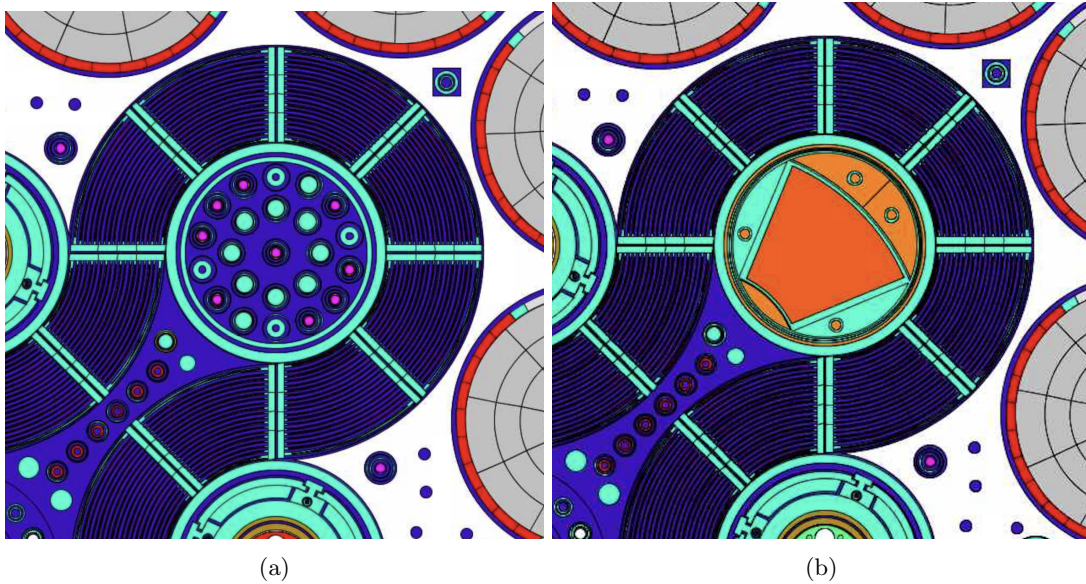


Fig. 2. Experiment loading in the ATR NEFT: (a) LIHA and (b) homogenized MURR-DDE (homogenHf configuration).

III.C. Analysis

Photon heat generation rate (HGR) tallies for each configuration were collected on a small assortment of nearby ATR positions, including the East Flux Trap (EFT), A-1, A-9, B-1, and I-21. The tallies for each experiment position included all the components contained within the full axial length of that position. This served as a basic average for each position. Each experiment position tallied contained aluminum fillers, with the exception of the EFT which was mostly aluminum and a small amount of low Z material. Among the additional tallies were a birth region filter of photons from the fueled regions on the same assortment of positions and a 3-D mesh tally of photon HGRs. The mesh tally was slightly larger than an ATR azimuthal quadrant that encapsulates the North Flux Trap, Center Flux Trap, and EFT—with a mesh size of 0.25 x 0.25 in. azimuthally x 1 in. axially. Fig. 1 shows the range of ATR positions for the photons and birth region filter HGRs.

Each of the modeled configurations was analyzed using exactly the same reactor driver fuel loading and control configuration, though with an important limitation placed on the results. Because the ATR can operate different lobe powers simultaneously, the amount of fuel needed to last the duration of the cycle normally varies from one lobe to the next and one cycle to the next. It stands to reason that a cycle with a highly reactive experiment inserted into one of the lobes would require less ATR fuel loading to maintain a specific lobe power than a less reactive experiment under identical conditions. Addressing this limitation would be very tricky, requiring many different ATR fuel loadings and control positions, ultimately bringing the applicability of the result comparison into question.

IV. RESULTS

The following results have all been generated with runs using 2^8 particles. The lobe power tallies have relative uncertainties of $<0.1\%$, HGR results have $<1\%$, and the photon birth region results of nearby fuel elements are $<3\%$. The axial data has been generated on quite a fine mesh and, as such, has uncertainties up to 10% . Although the errors associated with the mesh are fairly high, the size of the model necessitates unreasonably long run times to increase the statistics.

IV.A. Experiment Position Average

For each experiment position, all axial and radial components within the experiment were summed to produce a single average value for that position. These values are shown in Table II. Note: the HGRs between positions have not been compared since the volumes are different for each position.

TABLE II
Experiment photon HGRs for each configuration of the ATR positions [kW].

Configuration	B-1	A-1	A-9	I-21	EFT
liha	4.0	3.6	8.3	1.2	118.3
homogenHf	4.9	3.8	9.4	1.7	122.7
homogen	5.5	3.8	10.7	2.0	126.2
halfHomogen	4.9	3.8	9.9	1.7	123.4
halfDens	5.6	3.8	11.0	2.1	127.2
halfDensHalfLen	5.0	3.8	10.1	1.8	124.0
center	5.8	3.9	11.1	2.2	127.8
halfCent	5.1	3.8	10.2	1.8	124.3

Although these data show very small HGR changes for the ATR positions, a percent difference from the LIHA case was calculated to better understand the implications of these data. Table III shows these results, but keep in mind that the NE lobe power is not held constant and plays a significant role in the calculated values. In this table, the percent difference in the I-21 position is very large, but since it is outside the actively controlled portion of the ATR core, the magnitude is very low. As expected, the table shows that the positions very close to the NEFT (i.e., B-1 and A-9) register much larger changes, whereas those further away (i.e., A-9 and the EFT) show significantly less change. Another interesting observation is that the photon HGR values increased to a greater extent in the centered cases as opposed to the ones offset by +2.5 inches (the homogenHf, homogen, and halfHomogen configurations), suggesting there is a large dependence on the axial location.

To visualize how the ATR experiment positions differ in these configurations, the mesh tally data were used to create a heatmap, on which the ATR core internals and experiment positions were then overlaid. For the liha and homogenHf cases, the photon HGRs across the mesh at the core midplane are shown in Figs. 3(a) and 3(b), respectively. One sees a small increase in photon heating, mostly in the ATR driver fuel and the hafnium in the OSCCs. Fig. 4 shows the percent differences of these HGRs. Additional power generated by the lobe is pressed out toward the OSCCs. Bear in mind that although the percent differences are higher toward the outside (NE

TABLE III

Percent difference (to liha) in the experiment photon HGRs for each configuration [%].

Configuration	B-1	A-1	A-9	I-21	EFT
liha	0.0	0.0	0.0	0.0	0.0
homogenHf	21.5	3.4	12.9	38.3	3.7
homogen	35.8	5.5	27.6	66.5	6.6
halfHomogen	22.4	3.7	18.1	38.4	4.3
halfDens	38.6	5.8	32.0	74.4	7.5
halfDensHalfLen	24.0	4.0	20.9	44.7	4.8
center	42.8	6.5	33.5	83.0	8.1
halfCent	26.5	4.3	22.2	50.0	5.1

corner of each sub figure), the magnitude of heat is significantly lower.

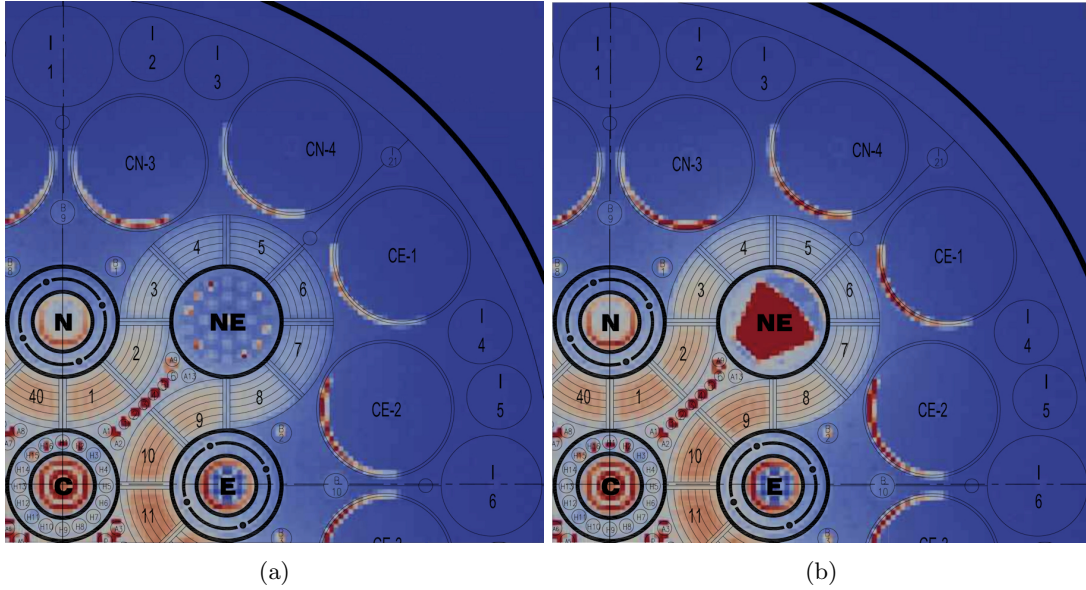


Fig. 3. Photon heat generation rate heatmap: (a) LIHA, (b) homogenized MURR-DDE (homogenHf configuration).

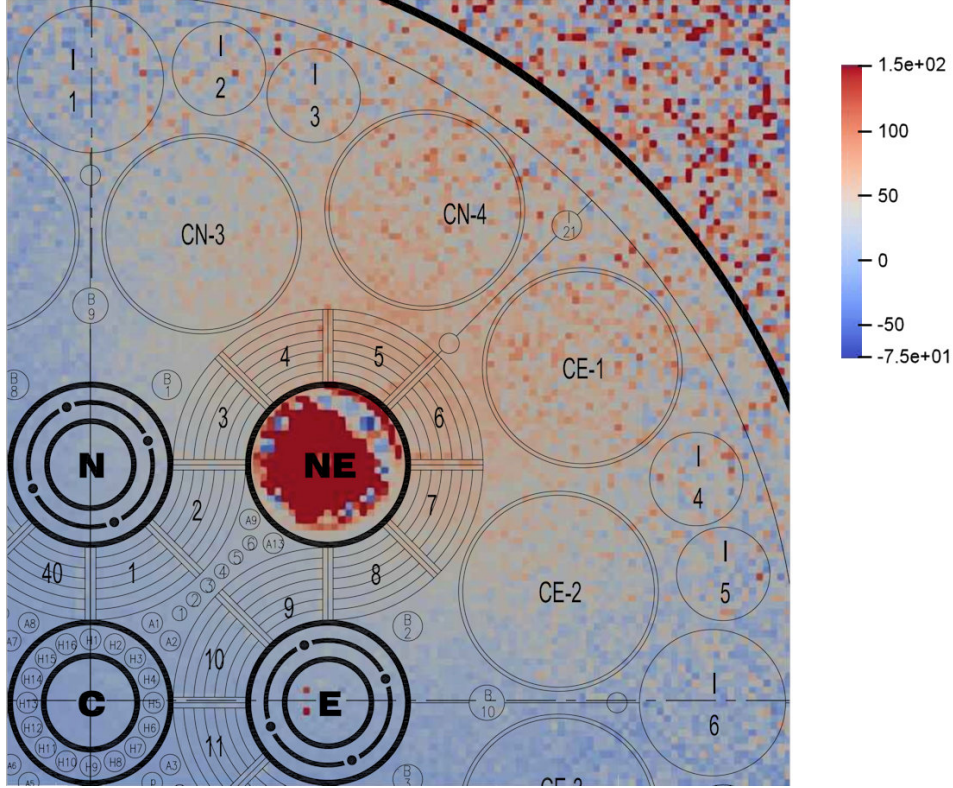


Fig. 4. Percent difference heatmap when comparing the liha and homogenHf configurations.

Table IV shows how the lobe powers are drastically altered by changing the configurations, and Table V shows their percent differences from the liha case. For the most part, the percent differences in the NE power do not align well with the percent differences in Table III for the experiment positions; however, another consideration must be made. All experiment positions except I-21 are in close enough proximity to get photon HGR contribution from another lobe. The I-21 position percent differences correlate well because most of the contribution stems from the NE lobe. Knowing that HGR is proportional to power, one sees that the large percent differences in photon HGRs are attributable—either wholly or in part—to the increase in NE lobe power.

IV.B. Photon Birth Regions

The ATR operating conditions of each configuration maintain similar OSCC positions, but adding the extra fuel in the modeled configurations dramatically alters the lobe powers of the core even though the total core power remains the same, as shown in Table IV. To better understand the effect each fuel element has on other experiment positions, a photon birth region filter was

TABLE IV

Lobe powers for each configuration, normalized to a total core power of 105 MW.

Configuration	NE	SE	SW	NW	C
liha	13.9	25.7	20.9	17.0	27.5
homogenHf	19.9	23.8	18.5	16.2	26.7
homogen	23.8	22.5	17.0	15.6	26.1
halfHomogen	19.7	23.8	18.5	16.2	26.7
halfDens	24.5	22.3	16.7	15.4	26.0
halfDensHalfLen	20.4	23.7	18.3	16.0	26.6
center	26.3	21.8	16.1	15.1	25.7
halfCent	21.4	23.3	17.9	15.9	26.4

TABLE V

Percent difference in the lobe powers for each configuration [%].

Configuration	NE	SE	SW	NW	C
liha.	0.0	0.0	0.0	0.0	0.0
homogenHf	43.4	-7.6	-11.5	-5.0	-2.9
homogen.	71.5	-12.4	-18.6	-8.7	-4.9
halfHomogen	42.5	-7.4	-11.3	-5.1	-2.8
halfDens	77.2	-13.2	-20.1	-9.4	-5.5
halfDensHalfLen	47.5	-8.0	-12.6	-5.9	-3.3
center	89.8	-15.3	-22.9	-11.2	-6.6
halfCent	54.6	-9.2	-14.3	-6.6	-3.9

used and tallied on the ATR fuel elements and the element in NEFT. By considering this birth region, one can understand the fractional contribution of the NEFT configuration to the photon HGR of the specific ATR positions.

Fig. 5 visualizes the fractional contributions of the homogenHf configuration. One sees that a large majority of the photons are generated in the ATR driver fuel elements. Predictably, the closer the experiment position to the NEFT, the higher the contribution from the homogenHf configuration's fuel element. One exception is the I-21 position, which is outside the actively controlled portion of the ATR and thus far from any fuel elements. In this case, the contribution from the homogenHf fuel element is roughly the same as the equiradial ATR driver fuel elements.

Finally, Table VI shows each NEFT configuration's percentage contributions of photon HGR on the ATR positions of interest. Since the liha configuration contains no fuel, there are no high-energy photons in this configuration to make it to the ATR experiment positions. Again, one sees that the experiment positions in close proximity to the NEFT, B-1 and A-9, have a higher contribution from the NEFT configuration than A-1 and EFT.

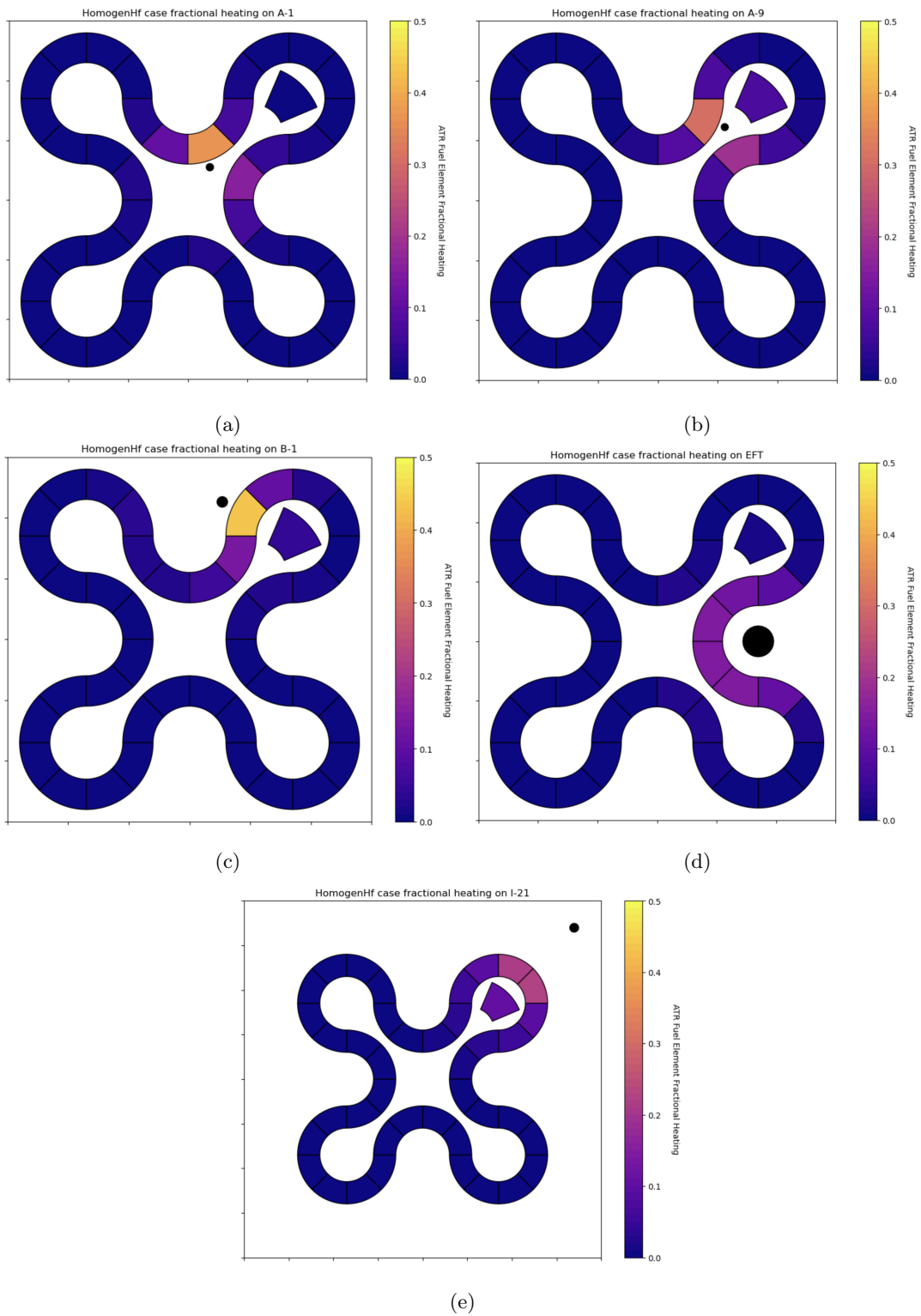


Fig. 5. Fractional contribution of the fuel in the homogenHf configuration on the ATR experiment position photon HGRs: (a) A-1, (b) A-9, (c) B-1, (d) EFT, and (e) I-21.

IV.C. Axial Effects

Both the KJRR and the MURR-DDE experiments are a different fuel length from the full ATR core axial length, creating the potential for change in the axial profile of the photon HGRs. The MURR-DDE experiment active fuel length is 24 inches, or half of the ATR actively fueled region. By considering configurations with changes in axial length, we can better understand these effects on other positions.

Fig. 6(a) shows a line scan of the HGR in an average of four mesh tally nodes in the azimuthal direction over the full axial length of the ATR. The liha case is notably lower in magnitude than the other configurations. Next, the homogenHf, homogen, and halfHomogen lines have a maximum that is slightly skewed above the core centerline, as is consistent with their axial locations from Table I. Fig. 6(b) shows the same information, but as a percent difference from the liha case. This plot makes it easier to see that the remainder of the cases also perturb the axial flux as a result of the homogenized fuel element not extending the full length of the ATR core.

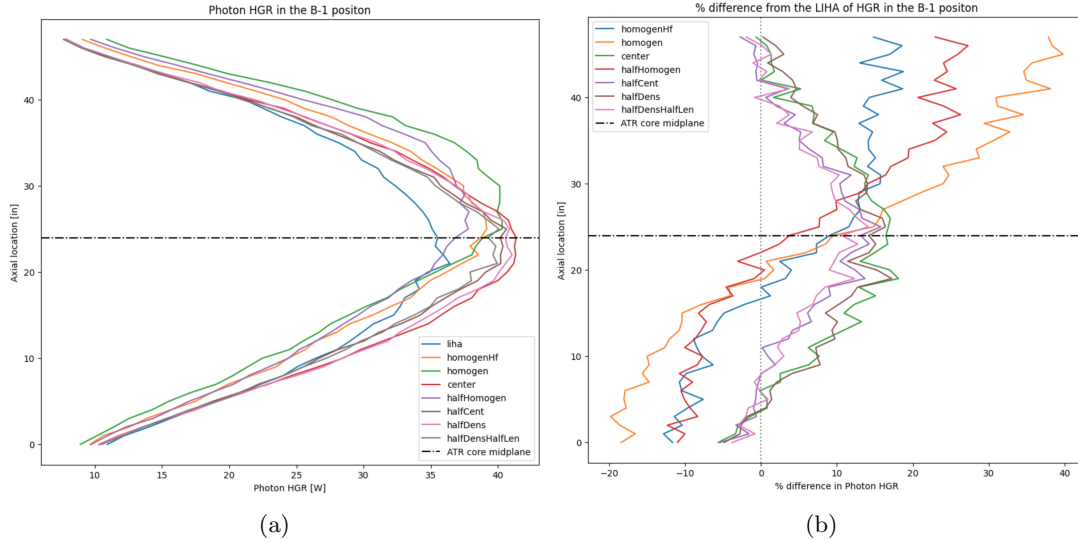


Fig. 6. Axial photon HGRs of the B-1 position: (a) HGRs and (b) % difference in HGR from the liha configuration.

Fig. 7 shows similar percent difference plots for the other four ATR positions. Notably, the axial results show a decreased HGR on the top and bottom edges, and an increased HGR at the core centerline. This suggests that the average increase in HGR reported in Table III does not tell the whole story. Although these results cannot show whether the configuration directly impacts

the heating rates, one can safely assume it does influence the surrounding driver fuel elements and in turn indirectly affects the axial heating shape in nearby experiment positions.

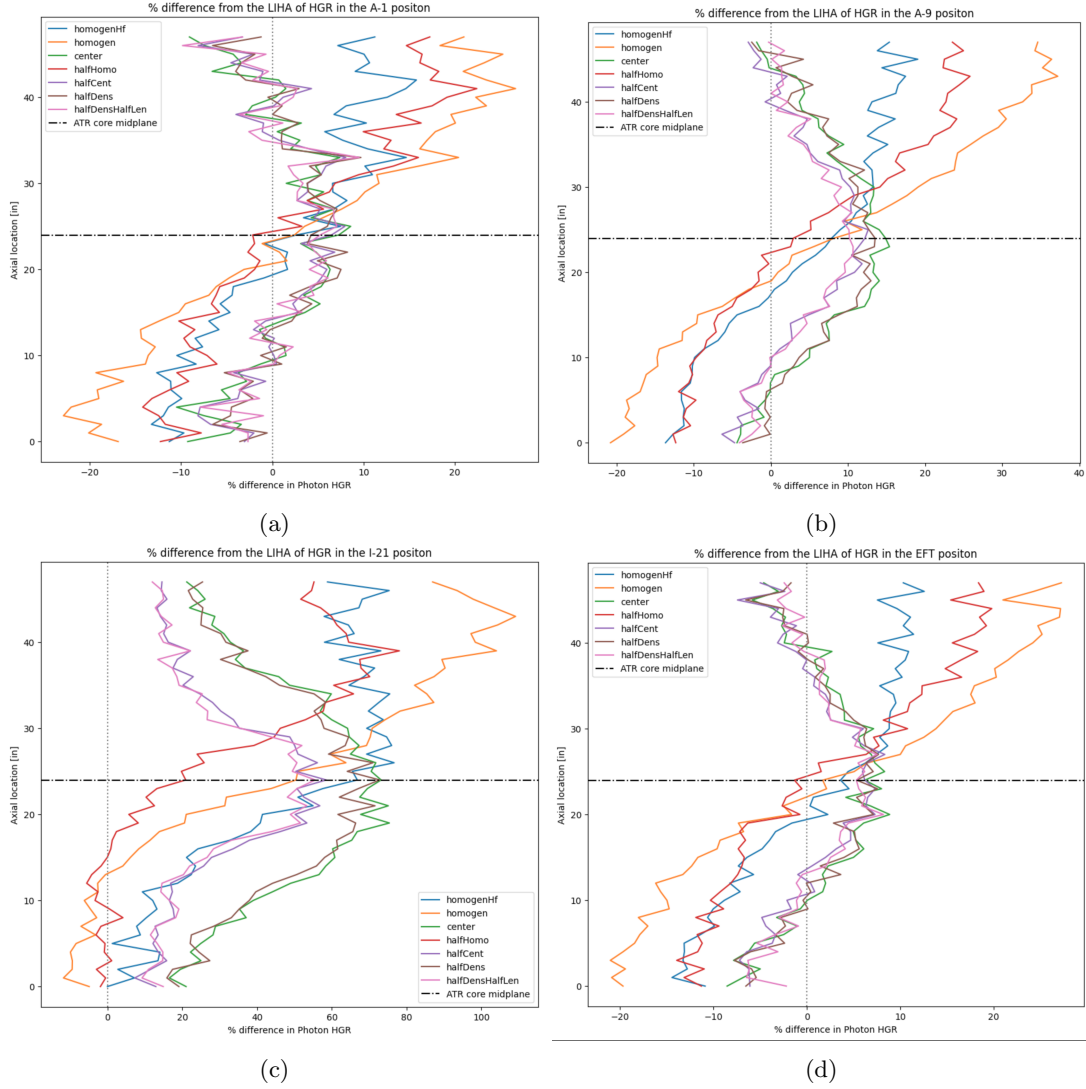


Fig. 7. Axial % difference in photon HGRs from the liha configuration: (a) A-1; (b) A-9; (c) I-21; (d) EFT.

V. CONCLUSIONS

The ATR's unique selection of experiment positions affords a wide range of irradiation conditions for advancing nuclear science and technology. In support of fuel qualification efforts pertaining to the HPRR Fuel Qualification Pillar, a highly loaded fuel element is planned for irradiation in

the NEFT and its photon HGR effects on nearby experiments have been explored. Additional configurations were also explored that may prove applicable to prospective experiments that have not been designed or analyzed yet.

The complex nature of the ATR driver fuel loading configuration used to maintain the lobe power distribution makes analyzing these effects nontrivial. When using the same reactor configuration, the ATR experiment position averages showed significant differences in photon HGRs, with those positions closer to the NEFT having the highest increases. These results were potentially biased because, as a result of keeping the reactor configuration the same, the power produced in the NEFT drastically increased. Since that is not how the ATR is typically operated, an effort was made to isolate the power effect, leveraging tallies of photon birth regions to examine the contribution from specific fuel elements. It was found that much smaller contributions from the positions' average photon HGRs could be attributed to the examined configurations, with less than 2% on the A-1 and EFT in the homogenHf case, as reported in Table VI. In general, the heating of high Z materials within a nearby experiment could have a more significant impact than the experiment initially planned. Additionally, experiments containing fuel could sustain less impact due to heat generation from within having a prevailing localized effect. Finally, the examined NEFT configurations did cause significant perturbations in the axial profile—a fact that should be an important consideration when planning nearby experiments.

ACKNOWLEDGMENTS

The authors wish to thank the U.S. Department of Energy (DOE) Material Management and Minimization program for their vital and continued support and funding of the High Performance Research Reactor Fuel Qualification Pillar at INL. This research made use of INL's High Performance Computing systems located at the Collaborative Computing Center and supported by the DOE Office of Nuclear Energy and the Nuclear Science User Facilities under Contract No. DE-AC07-05ID14517.

REFERENCES

- [1] S. BAYS, G. YOUINOU, M. LILLO, and P. GILBREATH, “ATR Compendium: Irradiation Test Capabilities,” *Nuclear Technology*, **201**, 3, 191 (2018); 10.1080/00295450.2018.1432967., URL <https://doi.org/10.1080/00295450.2018.1432967>.
- [2] C. MILLER, B. DURTSCHI, J. I. COLE, and K. DAUM, “U-10Mo Monolithic Fuel Qualification Plan,” (2021)URL <https://www.osti.gov/biblio/1781336>.
- [3] D. W. NIGG, J. W. NIELSEN, and D. R. NORMAN, “Validation of High-Fidelity Reactor Physics Models for Support of the KJRR Experimental Campaign in the Advanced Test Reactor,” ; 10.2172/1376195., URL <https://www.osti.gov/biblio/1376195>.
- [4] J. NIELSEN, “MC21 Benchmark of the Ki-Jang Research Reactor Experiment in ATR,” ECAR-4457, Idaho National Laboratory: Internal Document (2019).
- [5] J. BROOKMAN, “As-Run Physics Analysis for the AGC-4 Experiment Irradiated in the ATR,” ECAR-5345, Idaho National Laboratory: Internal Document (2021).
- [6] D. GRIESHEIMER, D. GILL, B. NEASE, T. SUTTON, and ET AL., “MC21 v.6.0 – A continuous-energy Monte Carlo particle transport code with integrated reactor feedback capabilities,” *Annals of Nuclear Energy*, **82**, 29 (2015); <https://doi.org/10.1016/j.anucene.2014.08.020>., URL <https://www.sciencedirect.com/science/article/pii/S0306454914004058>, joint International Conference on Supercomputing in Nuclear Applications and Monte Carlo 2013, SNA + MC 2013. Pluri- and Trans-disciplinarity, Towards New Modeling and Numerical Simulation Paradigms.
- [7] J. NIELSEN, “Base Model for the ATR MC21 Application,” ECAR-5030, Idaho National Laboratory: Internal Document (2020).
- [8] J. W. NIELSEN, “U-10Mo Conversion Burnup Benchmarking Activities for Full-Size LEU Fuel Plates,” URL <https://www.osti.gov/biblio/1478258>.
- [9] D. BROWN, M. CHADWICK, R. CAPOTE, A. KAHLER, and ET AL., “ENDF/B-VIII.0: The 8th Major Release of the Nuclear Reaction Data Library with CIELO-project Cross Sections, New Standards and Thermal Scattering Data,” *Nuclear Data Sheets*, **148**, 1

(2018); <https://doi.org/10.1016/j.nds.2018.02.001>., URL <https://www.sciencedirect.com/science/article/pii/S0090375218300206>, special Issue on Nuclear Reaction Data.

- [10] J. STILLMAN, E. WILSON, D. S. YOON, L. FOYTO, K. KUTIKKAD, J. C. MCKIBBEN, and N. PETERS, “Irradiation Demonstration Element Design Parameters for MURR LEU U-Mo Fuel Conversion,” ; 10.2172/1615245., URL <https://www.osti.gov/biblio/1615245>.

TABLE VI
 Percent contribution of each NEFT configuration on the ATR experiment positions.

Configuration	B-1	A-1	A-9	I-21	EFT
liha	0.0	0.0	0.0	0.0	0.0
homogenHf	4.1	0.8	7.5	10.1	1.6
homogen	4.8	1.0	8.9	10.7	2.1
halfHomogen	3.0	0.6	5.5	6.7	1.2
halfDensHalfLen	4.0	0.7	7.3	9.6	1.5
center	6.3	1.3	11.4	13.8	2.8
halfCent	4.2	0.8	7.6	10.1	1.7